Available online at www.sciencedirect.com
SCIENCE DIRECT®
Remote Sensing of Environment 87 (2003) 1–15
Remote Sensing of Environment
www.elsevier.com/locate/rse

Monthly burned area and forest fire carbon emission estimates for the Russian Federation from SPOT VGT

Y.-H. Zhang[a], M.J. Wooster[a,*], O. Tutubalina[b], G.L.W. Perry[a]

[a] Department of Geography, King's College London, Strand, London WC2R 2LS, UK
[b] Laboratory of Aerospace Methods, Faculty of Geography, Moscow State University, 119899, Vorobjevy Gory, Moscow, Russia

Received 19 December 2002; received in revised form 6 January 2003; accepted 22 May 2003

Abstract

Russian boreal forests contain around 25% of all global terrestrial carbon, some of which is released to the atmosphere when the forests burn. Whilst it is well known that fire is widespread in the boreal environment, there is a lack of good quality quantitative data on the extent of fire activity in Russian forests and on its interannual variation. This study provides one of the first comprehensive monthly satellite-based studies of fires occurring across the entire Russian Federation using a single, standardised methodology designed to map burned areas down to a size of 2 km^2. Using data from SPOT VEGETATION (VGT), we detect newly burned pixels via a series of multi-temporal spectral reflectance differencing criteria. For the year 2001, the method is applied to 21 VGT 10-day syntheses (S10) scenes covering the Russian fire season. We map 2764 fires with a total area of 41,782 km^2, and our methodology successfully detects all fires present in a comparison Landsat ETM+ data set, although it underestimates their size by on average of 18%. Using frequency–size relations, we estimate that 3790 fires of 1–2-km^2 area are likely to have remained unobserved by our method across the entire Russian region. Taking these corrections into account, we calculate the total burned area for the Russian Federation in 2001 as 51,546 km^2, with 38,512 km^2 occurring in forest and 13,034 km^2 in other land use classes. Fire activity is strongest in August in Eastern Siberia and the northern part of the Russian Far East, and in May and October in the southern part of the Russian Far East. Using these data, we estimate direct carbon emissions from these Russian forest fires to be 39.3–55.4 Mt, five to eight times that from the 2001 North American boreal forest fires and around 11–17% of that year's Russian industrial carbon emissions. This methodology will, in the future, be applied to the full VGT archive to quantify burned area and direct carbon emissions over a 5-year period in order to better assess the interannual variation in burned area and emissions and the relation to local climate.

Keywords: Russia; Forest fires; Burned area; Carbon; SPOT VGT

1. Introduction

Earth's boreal forests lie between 45° and 70°N and cover 9–12 million km^2, representing around one third of the total global forested area. It has been estimated that the vegetation, soils, and permafrost layer of the boreal zone represent around 37% of the total terrestrial carbon pool, and, therefore, the region is extremely important with regard to the Earth's carbon cycle (Goldammer & Furyaev, 1996). Approximately two thirds of Earth's closed boreal forest lies within the 17 million km^2 of the Russian Federation (Fig. 1), and this Russian forest represents around 25% of global terrestrial biomass (Conard et al., 2002; Kasisichke, 2000). Six factors control the storage and release of the boreal forest carbon: the rates of plant growth, biomass decay and permafrost formation, and the size, frequency, and severity of forest fires, which are the region's most dynamic disturbance factor (Fraser & Li, 2002; Kasischke, Christensen, & Stocks, 1995). Fire activity is believed to be particularly severe in parts of Western and Eastern Siberia and the Russian Far East (Conard et al., 2002).

Boreal forest fires induce a number of effects, each tending to release terrestrially stored carbon into the atmosphere. Firstly, the combustion of forest vegetation results in the short-term liberation of CO_2 in proportion to the area burnt and the type and density of biomass consumed. Secondly, the post-fire reduction in vegetation cover changes the radiation balance at the soil surface, leading to increased permafrost temperatures and potentially increased rates of soil decomposition for many tens of years of post-fire (Van Cleve, Oliver, Schlentner, Viereck, &

* Corresponding author. Fax: +44-2078-482577.
E-mail address: martin.wooster@kcl.ac.uk (M.J. Wooster).

0034-4257/03/$ - see front matter © 2003 Elsevier Inc. All rights reserved.
doi:10.1016/S0034-4257(03)00141-X

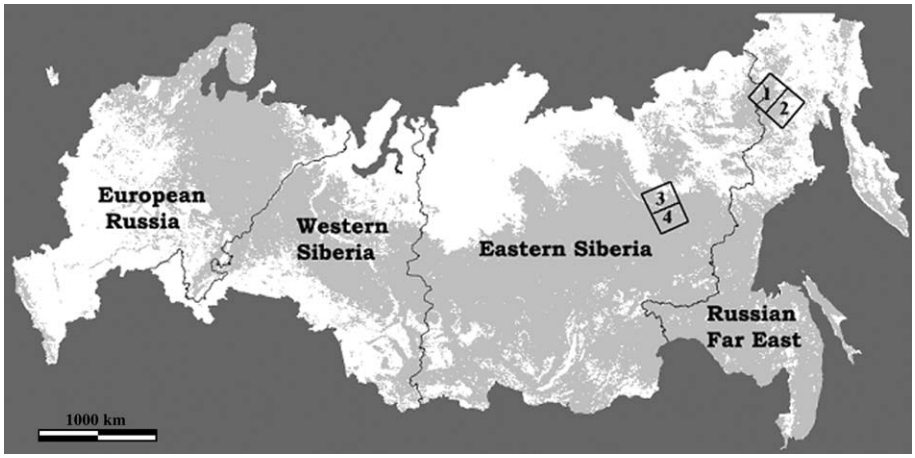

Fig. 1. The Russian Federation, which comprises around 11% of Earth's land surface area. Forest cover according to the USGS Global Land Cover Database (Anderson et al., 1976; Brown et al., 1999) is shown light in grey and covers 8.4 million km^2. The location of the four Landsat ETM+ scenes detailed in Table 2 are indicated.

Dyrness, 1983). Given the size of the boreal carbon pool, these effects mean that changes in boreal forest fire activity can have potentially significant effects on global atmospheric CO_2. It is therefore vital to know the annual area burnt in the boreal zone if current CO_2 flux levels are to be quantified and the effects of potential climate changes examined (Conard et al., 2002). This latter point is pertinent because it is predicted that any atmospheric warming related to increasing greenhouse gas concentrations will likely be most severe at higher latitudes, and that this could result in potentially significant increases in the annual fire affected area in the boreal zone through increases in vegetation flammability (Flannigan & Van Wagner, 1991). Indeed, in well-monitored areas such as Canada, there are already suggestions that the area burnt during the 1980s was significantly greater than that seen previously (Weber & Stocks, 1998).

Good quality data on burnt area in the entire North American boreal region are available for at least the last 50 years and show an interannual variability of an order of magnitude (Kasischke & French, 1995). However, for Russian forests, there is a lack of comparable data even for recent years, and this may well be the largest source of error in providing estimates of direct carbon release from the boreal region (Conard et al., 2002; Kasischke, Bourgeau-Chavez, O'Neill, & French, 2000; Wotawa, Novelli, Trainer, & Granier, 2001). Published estimates themselves vary enormously, with many of the smallest values being the official figures produced by agencies of the Russian Government (Conard & Ivanova, 1997; Conard et al., 2002). Satellite remote sensing appears as the only feasible, cost-effective method to collect systematic, quality-controlled data on fire activity over areas as large and as remote as those in Russia. Thermal, radar, and optical remote sensing has been used to detect both active fires and burnt areas in may different environments (e.g., Bourgeau-Chavez, Harrell, Kasischke, & French, 1997; Fuller, 2000; Justice, Malingreau, & Setzer, 1993), and several studies (e.g., Cahoon, Stocks, Levine, Cofer, & Barber, 1996; Conard et al., 2002; Stocks & Lynham, 1996) have used satellite imagery to measure burned area in individual Russian regions, yet, none has mapped the extent of fire activity over the entire Russian Federation. The most detailed study is that of Conard et al. (2002) who used AVHRR to estimate the total burned area for 1998 by mapping all fires larger than 10 km^{-2} in and around 30% of the Russian Federation outside European Russia. For the areas not covered by the AVHRR data, Conard et al. used adjustments to official statistics provided by the Russian Aerial Forest Protection Service. Analysis showed that for areas where both the aerial estimates and satellite images were available, the former underestimated burnt area by between 3 and 10 times. By adjusting the official statistics accordingly, Conard et al. were able to estimate the total burned area for the entire country and used this within a modelling strategy to estimate the carbon released during the 1998 forest fire events. Building on this important study, we adopt the emissions modelling methodology of Conard et al. but have extended the work in a number of areas: first, and most important, by mapping the burnt area over the entire Russian Federation using a single, standardised method; second, by using a satellite radiometer (SPOT VEGETATION [VGT]) having considerable technical advantages over the AVHRR (Saint, 1996) and which allows mapping of significantly smaller fires; and third, by providing monthly data on burnt area, rather than just an annual total, which substantially increases the capacity for comparing these data to other indices of fire activity such as observations of atmospheric pollutant products.

The remote sensing data that we use are from the VGT sensor onboard the SPOT-4 satellite, and we exploit these to provide the first published map of monthly forest fires in the Russian Federation for the 6-month 'fire season' of 2001, along with an estimate of the monthly

carbon emissions that result from these fires. In the future, we will apply the same methodology to the full VGT archive to quantify the interannual variability over a multi-year period so as to better quantify the importance of fires in the Russian boreal forest for the overall terrestrial carbon budget.

2. SPOT VGT characteristics for mapping burnt area

SPOT-4 was launched in March 1998, and the pushbroom VGT sensor provides imagery over a 2250-km swath width in the blue (0.43–0.47 μm), red (0.61–0.68 μm), near infrared (NIR, 0.78–0.89), and shortwave infrared (SWIR, 1.58–1.75 μm) spectral regions. VGT has a similar temporal resolution and nadir spatial resolution as AVHRR, but it shows significantly better performance with regard to geometric fidelity, radiometric calibration, multi-spectral registration, multi-temporal registration, and absolute geolocation (Saint, 1996; Stroppiana, Pinnock, Pereira, & Gregoire, 2002). VGT data are available in a number of different forms, including daily data of individual image swaths (primary data) and tiles of 10-day primary data syntheses covering fixed geographic regions (S10 data). For the S10 data, the selection of primary data image pixels is based on the maximum normalised difference vegetation index (NDVI) value occurring at each location over the 10-day compositing period, with the aim of providing a cloud-free mosaic for all areas of the globe every dekad (Passot, 2000). This strategy generally works quite well, but, in the cases of persistent cloud cover, it is inevitable that some cloud-contaminated observations persist in the S10 tiles, and, therefore, these must be removed or masked out during later processing.

Unlike AVHRR, the VGT sensor has no thermal channels and therefore cannot be used confidently to locate 'active' fires. However, VGT's excellent geometric and radiometric characteristics make it attractive for mapping burnt area (so-called fire 'scars'), and the strong potential of the VGT primary and S10 data for this application was demonstrated prior to launch by Eastwood, Plummer, Wyatt, and Stocks (1998). In-orbit performance with regard to fire scar mapping was subsequently studied by Stroppiana et al. (2002) for fires in Australia's tropical woodlands, and by Fraser and Li (2002) who investigated VGT as a partial replacement for AVHRR in the Hotspot and NDVI Differencing Synergy (HANDS) burnt area mapping methodology used in Canadian forests (Fraser, Li, & Cihlar, 2000). Ninety percent of the Russian Federation is included in the Northern Asia S10 data tile, produced by Flemish Institute for Technological Research (VITO), which covers all of the Russian Far East, Siberia, and part of European Russia. The Europe S10 data tile covers the remaining part of European Russia, and we use time series analysis of mosaics of the North Asia and Europe S10 data tiles to map Russian fires occurring during 2001.

3. Methodology for mapping burnt area in the Russian Federation

Our algorithm first creates a single monthly composite from the three S10 syntheses available each month. The seven monthly composites covering April to October are then used to map monthly burnt area in the 6-month May–October 'fire season.' For fires occurring in each month, the previous and current monthly composites are regarded as the pre- and post-fire images, respectively. This approach is clearly more data intensive than methods using just start- and end-of-season imagery to provide annual burned area totals (e.g., Fraser & Li, 2002; Fraser, Li, & Cihlar, 2000; Kasischke & French, 1995). However, we believe that our monthly methodology may well detect a greater proportion of burnt areas, particularly in areas of low-to-zero forest cover where regrowth of grassy vegetation may mask some fires that occurred early in the season. In any case, the provision of monthly data will improve investigations between fire activity and local climate variables and allows the derived emissions estimates to be better compared to simultaneous ground-based or satellite-derived atmospheric chemistry observations (Drummond, 1992; Oberlander, Brenninkmeijerm, Crutzen, Lelieveld, & Elansky, 2002).

Because NIR reflectance generally falls markedly on burning, the remote detection of newly burnt areas is commonly based on NIR reflectance thresholding, or observation of a significant NIR reflectance change (Fraser, Li, & Cihlar, 2000; Stroppiana et al., 2002). Investigation of spectroradiometric temporal changes occurring in the S10 data products, in concert with analysis of the USGS Global Land Cover Database (http://edcdaac.usgs.gov/glcc/glcc.html; Anderson, Hardy, Roach, & Witmer, 1976; Brown, Loveland, Ohlen, & Zhu, 1999) confirmed that a NIR reflectance decrease on burning does indeed occur for fires in all types of vegetation found in Russia. However, one important consideration is the fact that snow, ice, and frost frequently cover large parts of Russia, and the strong NIR reflectance of these surfaces can cause significant problems for the accurate identification of newly burnt areas. Specifically, major errors of omission can occur if a newly burnt area is covered by ice, frost, or snow between the specified pre-fire and post-fire image dates. Conversely, major errors of commission can occur when the snow, ice, or frost cover of an unburned region melts, resulting in a fall in NIR reflectance that may appear similar to that due to fire. To counter these effects, we use a NIR-minima criterion to create the monthly composites from the VGT S10 data. This criterion, which is similar to that employed by Fraser & Li (2002), has the effect of preferentially selecting composite pixels in their non-ice/snow/cloud covered state, and also selecting them in their burned state if they were subject to fire that month. A SWIR threshold equivalent to a reflectance of 8% was used concurrently to identify low NIR reflectance pixels that were due to cloud shadow, and not to burning, and therefore excluded

these from the compositing process. This SWIR threshold was determined via a training set of burned/unburned/cloudy regions.

The reasoning behind our methodology is demonstrated further in Fig. 2, which presents a NIR and SWIR spectral reflectance time series for two typical Russian forest areas, one that burns between 21 July and 1 August and another that remains unburned. The high NIR reflectance shown in (a) and the relatively modest SWIR reflectance shown in (b) for both areas in VGT data acquired before 1 May 2001 and after 11 September 2001 indicate heavy snow cover during these periods. For the burned pixel, a sharp fall in (a) NIR and (b) SWIR reflectance is observed between the S10 data labelled as 21/07 and 01/08, corresponding to the pre- and post-fire S10 composites, respectively. For the burned area, the most significant NIR and SWIR reflectance decrease outside of the April period of snow cover melting occurs coincident with the fire event (21 July to 1 August). The unburnt pixel shows no reflectance decrease at that time but does show significant decreases in NIR and SWIR reflectance at other times, but these have nothing to do with burning. The first occurs between 01/07 and 11/07, the second between 01/09 and 11/09, and both are caused by the appearance of surface ice or frost in the 01/07 and 21/08 S10 products. This increases the NIR and SWIR surface reflectance, and the subsequent melting causes the observed reflectance decrease in the S10 products.

Fig. 2c and d indicates how the decreases in NIR and SWIR reflectance observed in the July and September S10

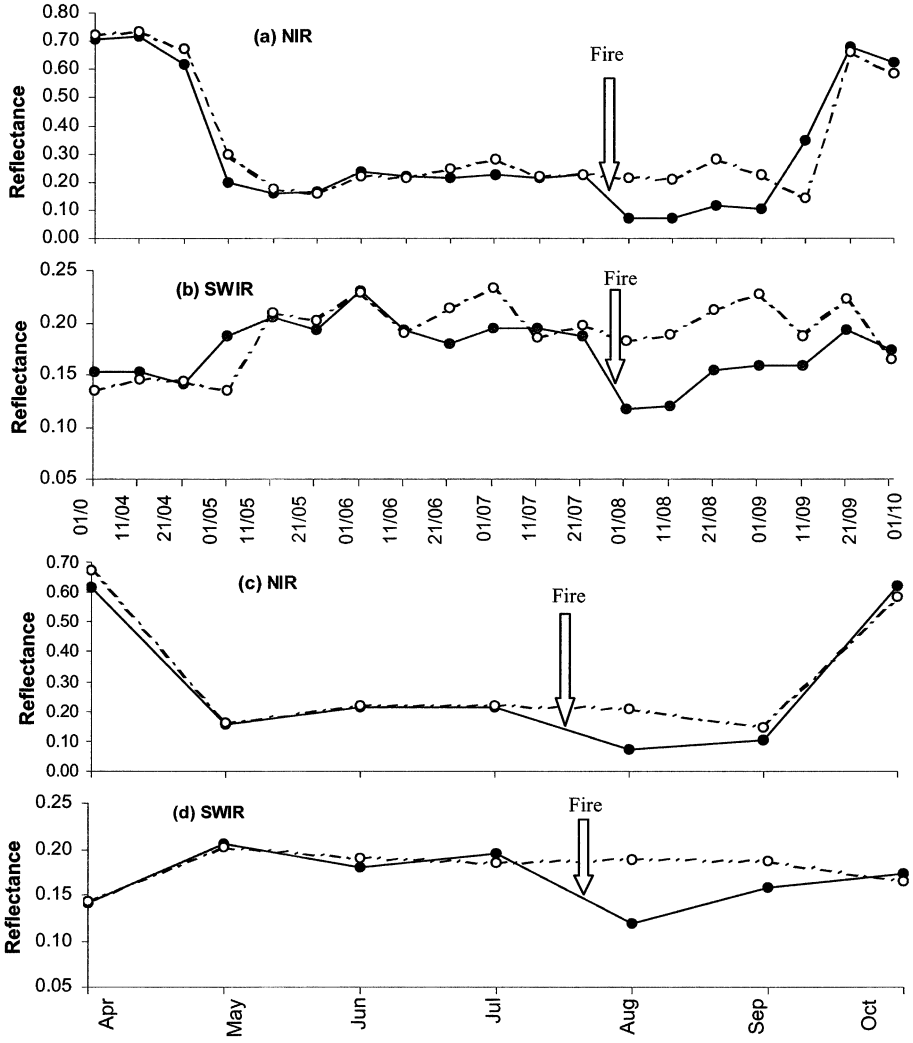

Fig. 2. April to October temporal evolution of the mean NIR and SWIR reflectance for two 15 × 15 pixel SPOT VGT data subsets located in the Russian boreal forest. One location (dashed line; 65.456°N, 158.705°E) is undisturbed by fire, whilst the other (solid line; 64.616°N, 157.036°E) suffered a fire between 21 July and 1 Aug 2001. Both areas are within Landsat ETM+ Scene 2, whose location is detailed in Fig. 1 and in Table 2. Panels (a) and (b) show the S10 NIR and SWIR reflectance data, respectively. The *x* axis captions in (b) denote the S10 product dates (e.g., 0401, 0411, 0421 are the S10 products for April). Panels (c) and (d) show, respectively, the corresponding NIR and SWIR reflectance from the monthly composites derived from the S10 data using the NIR-minima criterion. The *x* axis captions in (d) denote the date of each monthly composite. Note the different reflectance scales for the NIR and SWIR data due to snow having a much higher reflectance in the NIR than in the SWIR.

data of the unburned area are absent when we move to our derived monthly composites. This is because use of the NIR-minima criterion used to form the monthly composite excludes pixels with snow, ice, frost, or cloud cover if any of the three input S10 products have the pixel unaffected by these phenomena. In this way, the unburned areas are more likely to remain as a constant cover type in the monthly composite data, rather than undergoing the vegetation–ice/frost–vegetation cycle seen in the individual S10 products.

4. Algorithm details

As discussed in Section 3, a significant fall in NIR reflectance between pre- and post-fire image dates is regarded as our primary method for mapping burned areas with VGT. SWIR reflectance also decreases following a fire event, but we note that this often rapidly recovers a few weeks after burning, so that in some cases, only a small decrease in SWIR reflectance is observed between monthly pre- and post-fire SWIR data. This is demonstrated in Fig. 2c and d, where a 36% fall in SWIR reflectance occurs between the pre- and post-fire dates, compared to a 62% fall in the NIR reflectance.

Although Fig. 2 shows that a clear and ubiquitous NIR reflectance decrease accompanies burning, because other phenomena unrelated to fire also cause a similar NIR reflectance change we risk significant commission errors if we rely on this criterion alone to identify burned areas. Such phenomena include the residual appearance of ice, snow, or frost in the pre-fire image composites, which has melted in the post-fire image, residual cloud shadows that are present in the post-fire image but not the pre-fire image (i.e., partly shadowed pixels having erroneously passed the prior shadow-excluding processing) or the senescence of vegetation and fall-off of leaves from deciduous trees in the post-fire image. Further errors can occur due to the wide swath of the VGT sensor, which can lead to abnormally high reflectance observations at large viewing zenith angles due to surface BRDF effects (Stroppiana et al., 2002). This may cause problems if the pre- and post-fire data of a pixel were obtained at very different viewing geometries.

Although the phenomena outlined above may cause NIR decreases similar to that resulting from fire, further spectral analysis can help in discriminating 'true' burnt areas from these other effects. A training data set consisting of a minimum of 15 'true' fire scars per month, along with an approximately equal number of unburned areas suffering anomalous effects that caused rapid NIR decreases, was selected by visual analysis of pre- and post-fire VGT S-10 products. Examples of a pre- and post-fire training data subsets are shown in Fig. 3a and b, and analysis of these training data suggested that discrimination of 'true' from 'false' fire scars (mapped with the NIR decrease criteria) could be improved by using the VGT red and SWIR channels, along with two ratio-based indices; the NDVI and the shortwave infrared vegetation index (SWVI):

$$\mathrm{NDVI} = \frac{(\rho_{\mathrm{NIR}} - \rho_{\mathrm{red}})}{(\rho_{\mathrm{NIR}} + \rho_{\mathrm{red}})} \tag{1}$$

$$\mathrm{SWVI} = \frac{(\rho_{\mathrm{NIR}} - \rho_{\mathrm{SWIR}})}{(\rho_{\mathrm{NIR}} + \rho_{\mathrm{SWIR}})} \tag{2}$$

where ρ_{NIR}, ρ_{red}, and ρ_{SWIR} are the spectral reflectance recorded in the VGT NIR, red, and SWIR bands, respectively.

A series of additional threshold-based rules using pre- and post-fire red, SWIR, NDVI, and SWVI data were therefore generated to minimise commission errors with regard to burned area detection. In defining these rules, we noted that NDVI has previously been used to investigate monthly and annual burned area in various forest and grassland environments (Fredriksen, Lanaas, & Mbaye, 1990; Kasischke & French, 1995; Kasischke et al., 1993; Li, Nadon, & Cihlar, 2000; Martin & Chuvieco, 1993), whilst Fraser & Li (2002) found SWVI chnages between the start- and end-of-season to be an even stronger discriminator of burned forest in the Canadian boreal region. We did not utilise the VGT blue band because this provides little useful information on burned area (Fraser, Li, & Landry, 2000), but rather provides data of use to various atmospheric correction procedures (Kaufman & Tanré, 1992).

Our rules for the detection of burned areas are required to vary over the fire season because many of the phenomena that can be incorrectly identified as burned areas are active only at certain times, for example, melting of frost, ice, or snow or the falling of leaves. Table 1 details the full set of rules, and it should be noted that the threshold (T_i) used for each rule is temporally varying, its value being determined from the training data of that month. The training data were, as far as possible, distributed to fully cover the geographic locations and land cover classes encompassed in the Russian Federation and for each 'true' fire scar contained within the training data set the mean (M) and standard deviation (σ) of the reflectance and vegetation index values in both the pre- and post-fire images were calculated to define the threshold values. For Rules 1–5, the difference threshold T_i was determined from (3):

$$T_i = \min\{(M_{\mathrm{pre}} - 2\sigma_{\mathrm{pre}}) - (M_{\mathrm{post}} + 2\sigma_{\mathrm{post}})\} \tag{3}$$

For Rules 6–9, the absolute upper threshold T_i was determined using (4), whilst for Rule 10, the absolute lower threshold T_i was determined using (5):

$$T_i = \max\{(M + 2\sigma)\} \tag{4}$$

$$T_l = \min\{(M - 2\sigma)\} \tag{5}$$

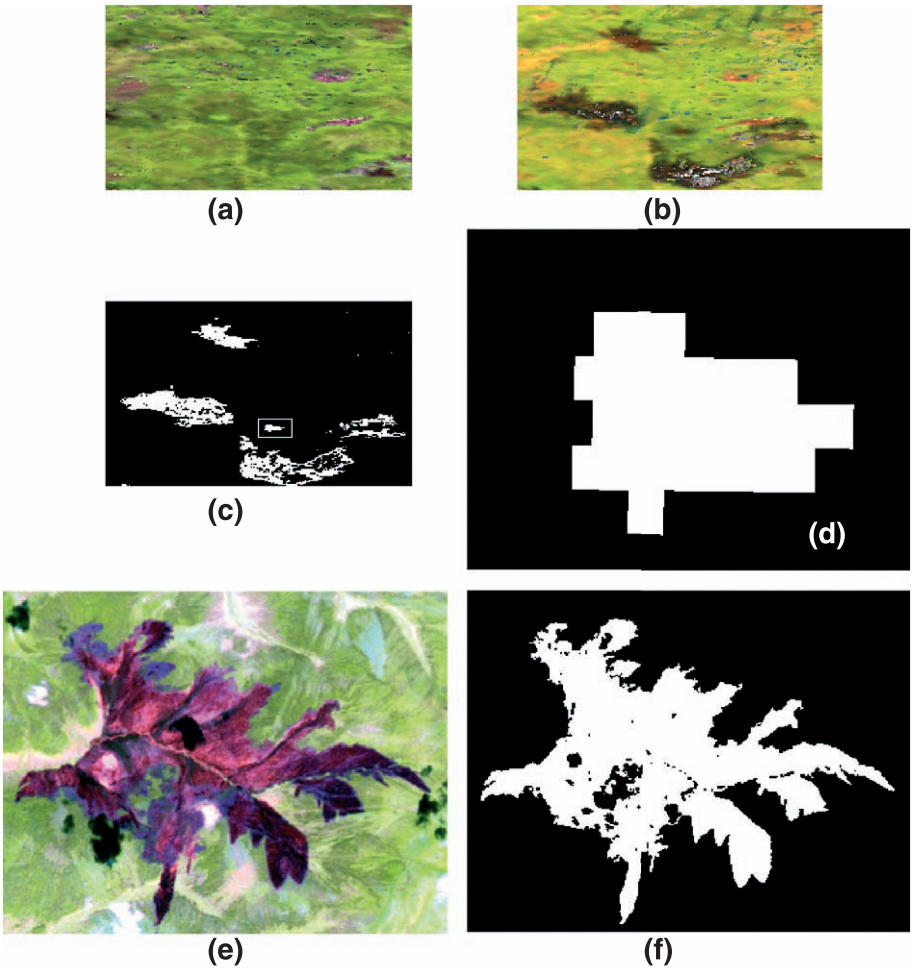

Fig. 3. (a) Pre-fire July 2001 VGT composite, (b) post-fire August 2001 composite, and (c) burnt areas detected from these two using the methodology described in Sections 3 and 4. All data are displayed in the original VGT Plate Carreé (latitude/longitude) projection and, in addition to the large burnt regions, six individual 1-km^2 areas have been detected as burnt but will be removed in the final processing step that removes spatially isolated pixels. One of the larger burns, having a VGT-derived area of 19 km^2 and outlined in (c) is displayed at increased magnification and in a UTM projection in (d). This fire is designated Fire 12 in Table 3 and (e) shows the corresponding area within the Landsat ETM+ data acquired soon after the fire on 18 August 2001 (Landsat ETM+ Scene 2; Table 2; Fig. 1), also displayed in a UTM projection. Panel (f) shows the fire scar derived from classification of ETM+ data, the area being 20.34 ± 0.50 km^2, with the uncertainty caused by the presence of several clouds and cloud shadows. All false colour composites are displayed as RGB = SWIR, NIR, red, showing burnt areas as dark in comparison to unburnt vegetation.

where min and max denote the minimum and maximum value over the entire training data set comprising true burned areas.

For each month under consideration, the algorithm works by first detecting potentially burned pixels using observed changes in NIR reflectance between the pre- and post-fire months (Rule 1). The additional rules active that month are then applied to test whether these potentially burned pixels are, in fact, burned, and this is confirmed if all rules are passed:

- Rule 3 (NDVI decrease) is not adopted for fires occurring in May and June (nor is it an absolute rule in July and August), because at these times, the monthly composite NDVI does not necessarily decrease but can actually increase after a fire. This is because, in some cases, the red reflectance decreases post-fire by a greater magnitude than the NIR reflectance, and this maybe related to the very rapid regrowth of new photosynthetically active vegetation in this warmer period.
- Rule 4 (SWVI decrease) is not used in the September–October period, because at that time, the SWVI decreases for many unburned areas due to vegetation senescence and falling of leaves in deciduous forests.
- Rule 5 (red reflectance decrease) is not adopted for fires in June and September (nor is it an absolute rule in July and August), but the reasons for this are different for each period. A decrease in red reflectance is commonly observed following fires, but during the summer months, burned areas sometimes become covered by sediment-laden melt-water, which can cause red reflectance to increase above the pre-fire value. Furthermore, for forest fires in September, a decrease in red reflec-

Table 1
Ten rules used in the identification and mapping of burnt area in the Russian Federation from SPOT VGT monthly composites

Rule	Month of pre- and post-fire image								
	April–May	May–June	June–July		July–August			August–September	September–October
1. $NIR_{pre} - NIR_{post} > T_1$	*	*	*	*	*	*	*	*	*
2. $SWIR_{pre} - SWIR_{post} > T_2$	*	*	*	*	*	*	*	*	*
3. $NDVI_{pre} - NDVI_{post} > T_3$			*		*		*	*	*
4. $SWVI_{pre} - SWVI_{post} > T_4$	*	*	*	*	*	*	*	*	
5. $RED_{pre} - RED_{post} > T_5$	*			*	*	*			*
6. $NIR_{pre} < T_6$	*	*	*	*	*	*	*	*	*
7. $SWIR_{pre} < T_7$			*	*	*	*	*		
8. $RED_{post} < T_8$	*		*		*	*	*	*	
9. $RED_{pre} < T_{11}$			*	*					
10. $MIN(NDVI) > T_9$		*						*	

The subscripts pre and post in Column 1 refer to the pre-fire and post-fire images, respectively, and T_i denotes the threshold used with each individual reflectance measure and vegetation index to discriminate burned areas. An asterisk in the monthly columns denotes that the test is applied in that month, and a pixel must pass all active tests if it is to be confirmed as a newly burnt area. June–July has two columns, denoting that there are two sets of fire scar identification rules used for burns occurring in this month, used with the logical OR relation. For the same reason, July–August has three rules, again used with the OR relation. Pixels confirmed as burnt are assumed to have burnt in the post-fire month.

tance is commonly unobserved in many newly burned areas.

• Rules 6–10 (NIR, SWIR, red, and NDVI absolute thresholds) are employed to minimise the effect of residual snow, frost, and surface water cover on the discrimination of burnt area. These absolute thresholds are extremely useful in reducing errors of commission due to the melting of frost and snow causing significant NIR reflectance decreases. Note that unlike Rules 6–9, Rule 10 is applied to both pre- and post-fire imagery.

It was found necessary to remove pixels corresponding to water bodies in the burned area maps resulting from the application of the above rules, because in some circumstances, water pixels can be mistakenly classified as burned areas. At the northerly latitudes considered here, many lakes and rivers become ice covered during the winter months, and when this ice melts, a major decrease in NIR reflectance results that can in some circumstances be incorrectly classified as due to fire. Large water features such as oceans and major lakes are already masked out in the S10 products, but rivers, coastal regions, and smaller lakes are not. To remove these water features, we use a land–water mask generated from the 30 arc-second Asia land cover data set produced by the Asian Association on Remote Sensing (AARS, 1999). After this step, each map of monthly burned area was converted from the original Plate Carreé (latitude/longitude) coordinate system into a Lambert Azimuthal Equal Area projection so that each pixel covered a fixed 1-km^2 area. Finally, any spatially isolated single pixels classified as burned were removed since, unlike the larger burned areas, many of these isolated pixels were seen to be due to residual artefacts of cloud shadow, sunglint, or the melting of frost, ice, or snow. Of course, any true 1-km^2 fires will also be removed by this step (which removed 8212 pixels in total), and this must be dealt with during any subsequent calculation of total burned area.

5. Validation

Following Fraser, Hall, and Landry (2001) and Smith, Wooster, Powell, and Usher (2002), the ability of the rule-based method described in Section 4 to accurately map burned area was tested by comparison to burned area maps derived from multi-spectral supervised maximum likelihood classification of Landsat-7 ETM+ imagery (Table 2). In total, 14 separate burns varying in size by two orders of magnitude were located and mapped using the ETM+ data, with the resulting burned area maps compared to our VGT-derived results. These burns occurred in deciduous needle-leaf forest, deciduous broadleaf forest, mixed forest, and wooded tundra, which are the land cover classes subject to severest burns in 2001 (as shown in Table 4). We can be sure that these were new rather than old burns because we were able to identify their date of formation using the VGT time series. Table 3 and Fig. 4 indicate that all 14 newly burned areas identifiable in the ETM+ data were successfully detected by VGT, but in all cases, Fire 1 aside, VGT underestimates the size of the burnt area by between 3% and 62%. This is because the rule-based method that we applied to the VGT data tends not to select all pixels on the perimeter of burned areas because many of these pixels will be dominated by unburned vegetation. The spectral reflectance characteristics of these particular "mixed" perimeter pixels prevent them being classified as burnt by our criteria.

Table 2
The four Landsat ETM+ images used for validation

ETM+ scene number	Path/ row	Upper left corner latitude/ longitude	Lower right corner latitude/ longitude	Date (dd/mm/yy)	Number of fire scars
1	104/14	66.62/156.45	64.51/161.72	18/08/01	5
2	104/15	65.25/155.32	63.18/160.43	18/08/01	5
3	122/15	65.28/127.64	63.16/132.50	16/06/02	3
4	122/16	63.88/126.54	61.80/131.27	03/10/01	1

Table 3
Burnt area estimates for 14 fires, determined via supervised maximum likelihood classification of Landsat ETM+ imagery and from SPOT VGT using the methodology described in Sections 3 and 4

Fire number	ETM+-derived area (km^2)	VGT-derived area (km^2)	Absolute area difference (km^2)	Relative area difference (%)
1	1681.92	1936	254.08	15.11
2	494.01	444	− 50.01	− 10.12
3	433.80	387	− 46.80	− 10.79
4	188.31	160	− 28.31	− 15.03
5	151.70	147	− 4.70	− 3.10
6	155.00	112	− 43.00	− 27.74
7	140.16	53	− 87.16	− 62.19
8	112.70	92	− 20.70	− 18.37
9	95.50 ± 6.00	75	− 20.50	− 21.47
10	31.67	25	− 6.67	− 21.06
11	25.60	20	− 5.60	− 21.88
12	20.34 ± 0.50	19	− 1.34	− 6.59
13	14.28	9	− 5.28	− 36.97
14	10.75 ± 1.00	5	− 5.75	− 53.49

For areas where the ETM+ image is contaminated by light cloud cover the appropriate uncertainty has been added to the ETM+-derived measurement. VGT underestimates burnt area by a mean of 17.6% (S.D. = 9.8%) if we discount the results from Fires 1, 7, and 14 (see text for discussion).

This is a markedly different result to that of Fraser et al., who found SPOT VGT to overestimate the size of burnt areas in Canadian forests by an average of 71% when compared to ETM+. It is possible that the method used by Fraser et al. selected a higher percentage of pixels containing sub-pixel bunt patches than did our method, though, conversely, this means that many of the 1-km pixels selected as burnt in the Fraser et al. study were, in fact, only partly burnt. This is something that is easily confirmed via comparison to the much higher spatial resolution ETM+ data. Actually, even at the 30-m scale, individual ETM+ pixels maybe comprised of a fragmented mosaic of burnt and unburnt patches, but at present, we have little very high resolution information (e.g., aerial photography) to assess this effect in Russian forests. In summary, the threshold values used in our rule-based procedure are set stringently to minimise errors of commission (i.e., to reduce 'false' fire scar detection) but with the disadvantage that fire-affected pixels containing considerable amounts of unburnt vegetation may quite frequently remain unidentified. This effect can, to some extent, be observed in Fig. 3, in which the VGT-derived product (Fig. 3d) appears to have missed the leftmost parts of the burn scar when compared to the ETM+-derived product (Fig. 3f). This, however, is counteracted by the fact that in many other regions of the burn, the ETM+ data confirms that the coarse 1-km^2 VGT pixels classified as 'burnt' are in fact a mix of burnt and unburnt areas. In this case, the final burnt area estimate derived from the ETM+ and VGT data sets differed by less than 2 km^2 (10%).

There is a particularly large underestimate (>50%) for the VGT-derived areas of Fires 7 and 14 in Table 3. The reason for this is that these two fire scars are crossed by a river, whose width in the AARS land–water mask is 90% greater than in the VGT imagery. Thus, some of the burnt pixels originally detected by our rule-based criteria are removed by the application of this mask, leading to an unusually large area underestimated by VGT in comparison to ETM+. The case of Fire 1 is also somewhat anomalous in that this fire scar is both extremely large (>1600 km^2) and is overestimated by VGT (Table 3). Examination of the VGT data shows that this fire burned over an unusually extended period, from July to September 2001, and whilst the ETM+ image was acquired soon after the cessation of burning on 3 October 2001, it was more than 2 months since the start of the fire. It is therefore possible that some of the apparently vegetated patches internal to the burnt region and observed with ETM+ were in fact burned at the time of the VGT overpasses 2 months previously, but that over the summer months, herbaceous vegetation has started to regrow. Furthermore, 20 small lakes with a total area of 18 km^2, which are not included in the AARS land–water mask, are present within the burnt region, and whilst VGT pixels containing these lakes are recognised as burned by our algorithm, the ETM+ burnt area classification does not include them.

For fires other than 1, 7, and 14 in Table 3, there is a maximum disagreement in burned area derived from the two sensors of 36%, with the VGT-derived measure on average 18% lower than that of ETM+. Simple linear regression indicates a strong linear relationship between the VGT and ETM+ measures:

$$\text{Area}_{\text{VGT}} = \text{Area}_{\text{TM}} \times 0.884,\ r^2 = 0.995,\ P < 0.005 \quad (6)$$

for Fires 2–6 and 8–13 in Table 3

$$\text{Area}_{\text{VGT}} = \text{Area}_{\text{TM}} \times 0.866,\ R^2 = 0.975,\ P < 0.005 \quad (7)$$

for all Fires in Table 3 except Fire 1.

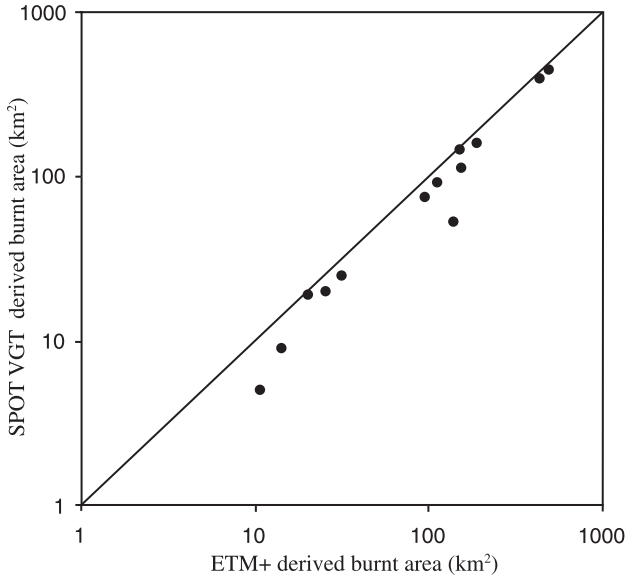

Fig. 4. ETM+- and SPOT VGT-derived burnt area for Fires 2–14 of Table 3. The 1:1 correspondence line is shown and VGT underestimates burnt area in all cases shown.

Whilst the ETM+ data used in the validation effort do encompass the land cover classes most severely affected by fire in 2001, it is clearly the case that increased confidence could be placed in the validation procedure if the number of ETM+ scenes used was increased and was able to cover all the affected land cover classes. This, however, is difficult because of the limited number of ETM+ scenes available (usually three to six scenes each year for any particular location) and the fact that many scenes are corrupted by cloud and ice/snow cover. We have checked another 12 ETM+ quicklook (240 m) resolution scenes containing 40 additional fire scars (in the same land cover classes as the four validation ETM+ images). An example of this comparison is shown in Fig. 5, and comparison between these ETM+ quicklooks and the VGT-derived fire scar map indicates that VGT detected 98% of the burned areas present in the quicklook imagery, with the missed scars having areas 1 km^2 or smaller. In general, as with the previous validation data set, the VGT mapped fire scars again appear smaller than they do in ETM+. We plan to adopt Landsat TM and ETM+ imagery as the validation data for the remaining years of our study and to produce a much more comprehensive validation report, covering aspects of fire timing, position, and burned area land cover, along with confirmation of the hypothesis that the degree of area under- or overestimation is a function of fire scar size.

Once the accuracy assessment of the resulting VGT-derived burned area maps was complete, the rule-based methodology was applied to the full set of monthly VGT composites of the Russian Federation for the 2001 fire season (April–October), providing monthly burned area maps from May to October. The final map of annual burnt area is simply the union of each individual monthly map.

6. Results

6.1. Burnt areas mapped in 2001

Fig. 6 shows the map of burnt area for the entire Russian Federation, whilst Fig. 7 shows parts of the most fire-affected region of Eastern Siberia in more detail. It is apparent that the distribution of fires in Russia is extremely nonuniform, with the early- and late-season burns (fires in May and October) located mainly in the south of Russia, especially in Novosibirsk Oblast, the Republic of Khakassia, Chita Oblast, Amur Oblast, Khabarovsk Kray, and the Yevreyskaya Autonomous Region. Mid-season fires occur mainly in areas of Eastern Siberia and the northern parts of the Russian Far East, particularly the Republic of Sakha, the Chukchi Autonomous District, and Magadan Oblast.

Differentiating between burns with regard to detailed vegetation type obviously requires use of a land cover classification scheme. The most important class distinction for our work was forest/nonforest, and there are three land cover products providing this information for the entire Russian Federation: the Russian Resource Atlas (http://www.iiasa.ac.at/Research/FOR/russia_cd), the USGS Global Land Cover Characteristics Database (http://edcdaac.usgs.gov/glcc/glcc.html), and the Forest Resources Assessment

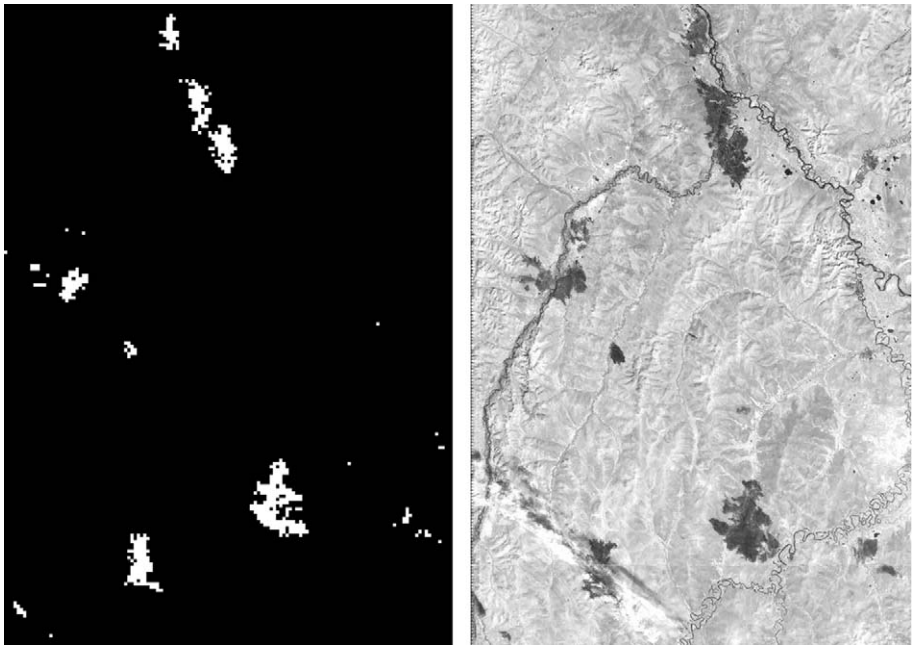

Fig. 5. SPOT VGT-derived fire scar map for August 2001 (left) and ETM+ quicklock image of 16 August 2001 (right) in which burnt areas appear dark. Both data sets are displayed at the same scale and the image fragments cover a ground region of approximate size 130 × 190 km. Cloud (white) is seen in the bottom left of the image and covers part of large fire scar located there. The comparison suggests that SPOT VGT has detected all burnt areas larger than 1 km^2 present in ETM+ image but has tended to underestimate their size.

Fig. 6. Burned area across the Russian Federation for 2001 as mapped from SPOT VGT. The majority of fires occurred in May, August, and October in Eastern Siberia and the Russian Far East, though fires also occurred in Western Siberia and European Russia. The boxed areas are shown in more detail in Fig. 7, along with the fires temporal distribution. Data are displayed in a Lambert azimuthal equal area projection and the boundaries of the individual Administrative regions are shown.

2000 (http://www.fao.org/forestry/fo/fra). Each of these products employs a different classification scheme, but each can be collapsed to a simple forest/nonforest grouping. We compared the areas of forest class for each scheme and found the USGS scheme to report a median value of 8,449,607 km^2, with the Russian Resource Atlas almost 10% higher (7,635,433 km^2) and the FRA 2000 almost 10% lower (9,144,058 km^2). For this reason, we

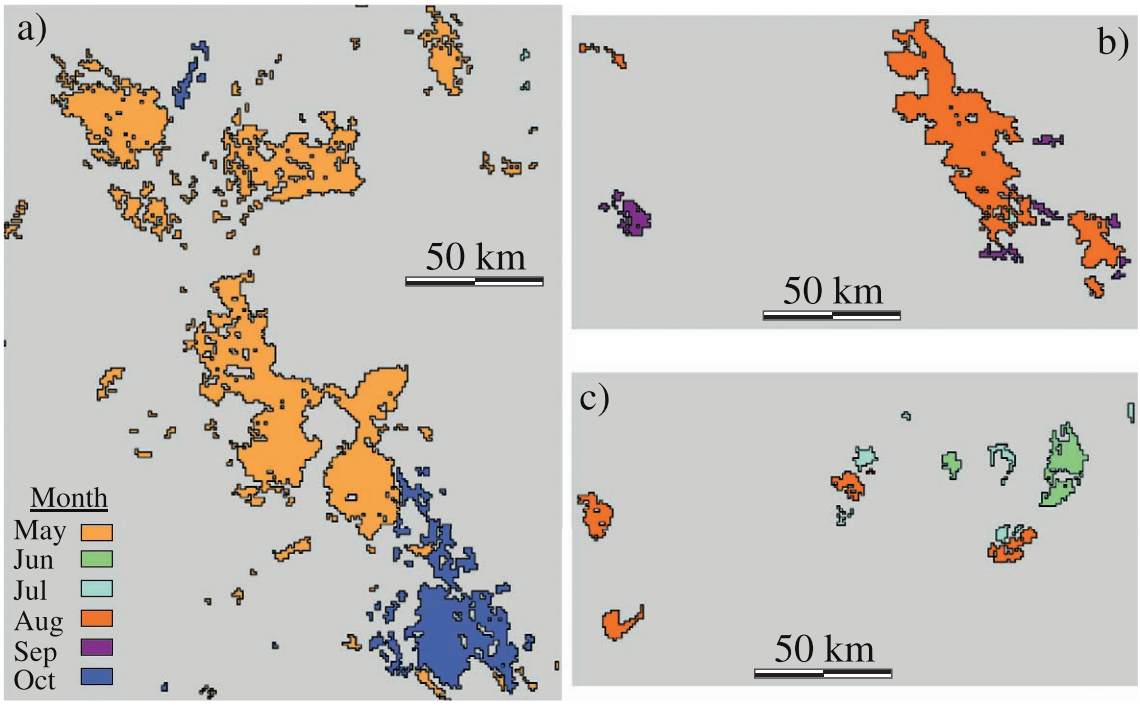

Fig. 7. Increased detail for the three boxed areas delineated in Fig. 6 (bottom to top). The colour scheme in (a) is used to represent burns occurring in different months, and fires occur throughout May to October 2001. The largest burnt areas mapped in 2001 are shown in (a) whilst the large burn in (b) is the longest-lived fire (Fire 1 in Table 3), which burnt for 3 months (July–September). Fires mapped in different months are outlined in black to aid interpretation and burnt areas mapped in each of the months in which fires were detected are shown.

chose the median forest cover area reported by the USGS land cover classification scheme, and Table 4 reports our VGT-derived burned area statistics by both month and land cover type in relation to the USGS land cover database. From May to October 2001, the total burnt area mapped with a minimum patch size of 2 km^2 was 41,896 km^2 across the whole of the Russian Federation. Seventy-five percent (31,313 km^2) of this burning occurred in forest classes, with the remaining 25% (10,583 km^2) affecting nonforest classes. If the six individual monthly maps of burnt area are overlain, then the resulting burnt area total is slightly lower than the total of the individual monthly maps, at 41,782 km^2; the difference being due to burning being detected repeatedly within the same pixels for several months. August is the month in which the majority of burning occurs, mainly in deciduous forests, but more surprisingly May and October have burned area totals within 25% of that occurring in the August peak, though mainly in mixed forests or steppes (which in this environment are essentially grasslands with sparse tree cover or intermixed forest and grass/croplands). Table 4 shows that far fewer fires took place in June, July, and September than in August, May, and October.

6.2. Fire size and frequency relations and total burned area

We detected 2764 separately burned areas in 2001 having 141 different fire sizes, with the largest being a 4063-km^2 fire occurring near the Russia–China border in east-southern Russia and which burned mainly steppe and mixed forest. The frequency–size distribution of the fires detected by VGT can be analyzed with reference to Bak, Tang, and Wiesenfeld (1988) who developed the concept of self-organized criticality (SOC) to model and describe the behavior of certain extended dynamical systems. Malamud, Morein, and Turcotte (1998), Malamud and Turcotte (2000), and Ricotta, Avena, and Marchetti (1999) studied the so-called self-organized criticality of both real and modeled forest fires and found that the cumulative frequency vs. area distributions are well fitted by power laws, manifested by a linear relationship of log (cumulative frequency) against log (area), where the cumulative frequency (N_{cf}) is the number of fire scars having area greater than A_f. We analysed the occurrence frequency of the 141 differently sized fires mapped from VGT and found the relationship is also well fitted by a power law, in this case having an exponent of 1.03 (Fig. 8). Comparison between our relationship and those presented by Malamud et al. (1998) suggests that our measured frequency–size distribution is similar to those of other forest fire regimes, whilst the exponent value close to 1.0 means that small and large fires contribute roughly equally to the total area burned (e.g., fires of area A occur roughly two orders of magnitude more frequently than fires of size 100A, so both contribute roughly equally to the total burnt area). Table 5 shows the mapped forest fires categorized into four size classes, indicating that in the case of the 2001 fires mapped by SPOT VGT, the 9 largest files and 2497 smallest fires contribute almost equally to the total burnt area. However, the extreme size of the largest fires means that the largest 1% of fires contribute 42% of the total area burned.

In addition to the above analysis, the key use of the power law shown in Fig. 8 is that it allows us to predict how many individual fires burning less than 2 km^2 are likely to

Table 4
Burnt area for the Russian Federation in 2001, classified by land cover as expressed in the USGS Global Land Cover Database using the USGS land use and land cover classification legend (Anderson et al., 1976; Brown et al., 1999; http://edcdaac.usgs.gov/glcc.html)

	Land cover class	Land cover area (km^2)	May	June	July	August	September	October	Area burned (km^2)	Total burned in 2001 (km^2)
Forest	Steppe	637 835	4496	69	42	725	24	1224	6580	31 313, 31 217
	Deciduous broadleaf forest	1 390 044	43	235	1062	5052	209	85	6682	
	Deciduous needleleaf forest	1 908 367	1409	467	375	3364	919	691	7225	
	Evergreen needleleaf forest	1 195 125	39	24	16	25	3	27	134	
	Mixed forest	3 318 235	4215	122	109	960	124	5158	10 688	
Nonforest	Urban and built-up land	38 401	8	0	0	9	0	5	22	10 583, 10 565
	Dryland, cropland and pasture	1 468 938	685	19	33	245	10	2719	3711	
	Irrigated cropland and pasture	61 148	46	6	5	37	2	26	112	
	Cropland/grassland mosaic	735 673	203	4	40	128	0	171	546	
	Cropland/woodland mosaic	667 369	3	2	22	62	7	66	162	
	Grassland	240 643	490	34	1320	517	23	29	2413	
	Shrubland	259	0	15	40	269	5	1	330	
	Herbaceous wetland	28 194	87	13	16	92	9	16	233	
	Wooded wetland	546 778	1	73	13	655	20	8	770	
	Wooded tundra	3 061 148	0	131	388	1479	199	9	2203	
	Mixed tundra	548 873	0	0	5	50	16	0	71	
Total			11 725	1214	3486	13 666	1570	10 235		41 896
Annual area burned (km^2)										41 782

Note that the term *steppe* has been used in place of *savanna* due to its more widespread usage in describing characteristic high-latitude environments. In the final column, the two figures for total area burned in the forest and nonforest classes are derived respectively by summing and overlaying the monthly maps, the latter providing a slightly lower estimate, because in a few cases, fires burned the same region repeatedly for more than 1 month.

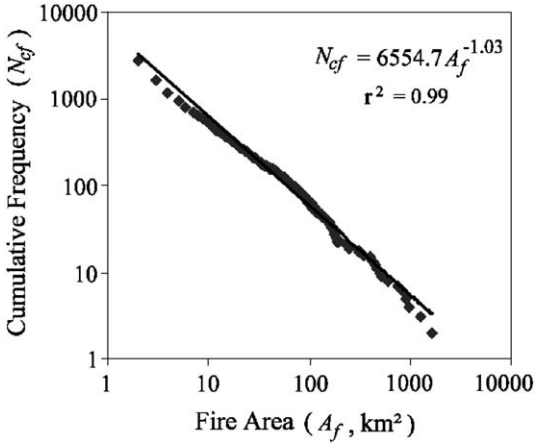

Fig. 8. The frequency–magnitude relationship of fires mapped by SPOT VGT. The data are well fitted by a power law distribution with an exponent close to 1.0.

have occurred in 2001 and yet were not mapped by our methodology (which limits detection to fires of area 2 km^2 or greater). The prediction is that there will be 6554 fires larger than 1 km^2, and because our VGT-based methodology maps 2764 fires larger than 2 km^2, we estimate that 3790 fires having an area of 1–2 km^2 have been missed by our SPOT VGT-based method. We do not predict the likely number of fires smaller than 1 km^2 because Ricotta et al. (2001) indicate that different processes maybe controlling the frequency and size of these sub-kilometer scale fires than are controlling the larger fires typically observed by VGT, meaning extrapolation of the power law to fires much smaller than those observed could produce highly inaccurate estimates. According to results shown in Ricotta et al., the frequency of the very smallest fires will, anyway, be significantly lower than that predicted by extrapolation of the frequency–size distribution, further supporting the decision to neglect them from the analysis.

Using these frequency–size data, we estimate the actual area burned in the Russian Federation for 2001 to be 41,782 km^2 (measured) and 3790 km^2 (predicted); making a total of 45,572 km^2, of which 75% occurred in forests. Using Eq. (6) to account for the apparent underestimate of burnt area by VGT when compared to ETM+ provides the final corrected burnt area estimate of 51,546 km^2, with 38,512 km^2 in forest and 13,034 km^2 in nonforest. This equates to 0.5% of the total area of forest recorded in the Russian Federation by the USGS Global Land Cover Database (Table 4; Brown et al., 1999).

Table 5
Burn areas for 2001 categorised into four size classes

Size category of burned area (km^2)	Total area burned		Number of individual burned areas	
	km^2	%	*n*	%
≤ 20	10755	25.79	2947	90.34
>20 to ≤ 100	19907	21.86	204	7.38
>100 to ≤ 500	30207	24.65	54	1.95
>500	11575	27.70	9	0.33
Total	41782	100	2764	100

7. Carbon emission estimates

We used our measurements of monthly burned area to estimate the direct carbon emissions from the areas of Russian forest burned in 2001. Isaev et al. (2002) and Redmond, Winne, Opitz, and Mangrich (2002) provide recent evidence that the severity of the burn may itself be detectable from remote sensing. However, whilst very promising, these techniques are new and currently have only been applied to high spatial resolution imagery. It remains to be seen whether detailed testing can prove that similar approaches applied to low or moderate spatial resolution data will allow burn severity to be mapped over the full range of environmental conditions found across Russia. In the absence of such a remote sensing approach, we follow other recent studies by assuming a range of possible burn severities to estimate the minimum and maximum levels of carbon emission from the 2001 fires. Specifically, we follow Conard and Ivanova (1997) and Conard et al. (2002) in examining two scenarios, that burns during the season were dominated by severe burning conditions (50% of burnt area in crown fires, 30% in moderate-severity surface fires, and 20% in low-severity surface fires) or moderate burning conditions (20% crown fires, 60% moderate-severity surface fires and 20% low-severity surface fires). Conard et al. (2002) report that mean levels of carbon emission for crown fires, moderate-severity surface fires, and low-severity surface fires are respectively 22.5, 8.6, and 2.3 Mg/ha, based on weighted carbon storage in different biomass and forest litter components (Alexeyev & Birdsey, 1994; Alexeyev, Birdsey, Stakanov, & Korotkov, 1995). Using these data with our VGT-based measurements allows us to estimate carbon emissions over the 2001 fire

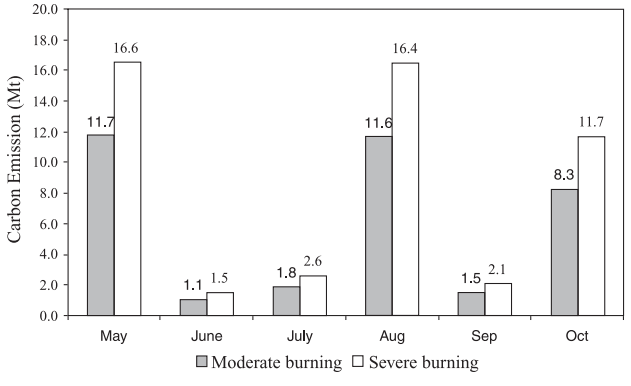

Fig. 9. Monthly direct carbon emissions (million tonnes) due to boreal forest fires occurring across Russia in 2001, calculated from VGT measurements of burnt area and assuming fire intensities were those of a moderate burning season (minimum emissions) and a severe burning season (maximum emissions). Additional carbon emissions of 3.3–4.6 Mt (annual total) are estimated due to smaller forest fires unobserved by VGT.

season on a monthly basis (Fig. 9). Note that the correction factor derived from comparison between the VGT burnt area map and the ETM+ data has been applied to our VGT measurements of monthly burned area shown in Table 4 and that we include only areas of burnt forest in the calculation. Calculated carbon emissions for 2001 related to forest burning are 36.0 Mt for the moderate burning scenario and 50.8 Mt for the severe burning scenario. Given the climate prevalent in 2001, it seems more likely that moderate burning conditions predominated. Using the frequency–size distribution results, we can also calculate the additional carbon emissions that would be contributed by the 3290 fires of size 1–2 km^2 that remained undetected by VGT, and this provides an additional 3.3 and 4.6 Mt to the moderate fire severity and high fire severity calculations, respectively. This means that total carbon emissions from direct forest fires across Russia in 2001 are estimated between 39.3 and 55.4 Mt. Additional carbon emissions associated with non-forest burns mapped from VGT increases these estimates by 4–6%, assuming that the emissions per unit area for these nonforest fires are equivalent to those of low-severity surface fires.

For comparison, the Canadian Interagency Forest Fire Centre (Johnston, 2001) reports that for Canada in 2001, a total of 7173 fires burned 6298 km^2 of forest, whilst the Alaska Division of Forestry (2002) reports 321 fires burned 400 km^2 of Alaskan forest. Therefore, in 2001, the total burned area of forest in the North American boreal region is only 17% of that burned in the Russian Federation. Again adopting the methodology of Conard et al. (2002), who assume a greater crown fire incidence in North America (80% and 90% of fires in the low-severity and high-severity years, respectively, with the remaining fires as surface fires) and lower carbon storage per unit area (12.5 Mg/ha for crown fires and 7.0 Mg/ha for surface fires), we estimate direct carbon emissions from these North American fires as 7.6–8.0 Tg, equivalent to 14–19% of the Russian figures.

8. Conclusions

Using SPOT VGT data, this study provides the first comprehensive satellite surveillance of monthly burnt areas occurring in forests and other land use classes across entire Russian Federation. We detect 2764 separate burnt areas covering a total of 41,782 km^2, with 31,217 km^2 in forest land cover classes. The largest fire burnt 4063 km^2, whilst the longest-lived fire burned for 3 months. May, August, and October are the peak months for fire activity and the majority of fires occur in Eastern Siberia and the Russian Far East. Comparison of the VGT-derived burnt area maps to Landsat ETM+ suggests our methodology successfully detects burned areas of size 2 km^2 or greater, but underestimates their size (by on average 18%), reflecting our attempts to minimize errors of commission. Using frequency–magnitude analysis of the 2764 fires detected by VGT, we further estimate that around 3790 fires of area 1–2 km^2 may have been missed. Adjusting our VGT-based burned area estimate by these factors, we estimate a total of 51,546 km^2 burned in the Russian Federation in 2001, 38,512 km^2 in forest and 13,034 km^2 in other land use classes. Further comparisons to ETM+ data would clearly be advisable, but we believe that these figures are accurate to perhaps $\pm 25\%$. Whilst we believe this to be the most accurate and extensive burned area estimate yet available for the Russian Federation, it is clear that some improvements could be made to the methodology, for example, an enhanced land–water mask could be used (perhaps derived from the VGT imagery itself) because the current mask can remove burned areas occurring along rivers. Furthermore, VGT imagery from the previous October and current April could be used as the pre- and post-fire image to detect any fires that occur before the current fire season commences. Finally, the use of multi-year imagery will allow assessment of forest areas that burn repeatedly due to the dryness and flammability of the previously burnt vegetation and soils, these fires having carbon emissions per unit area that may deviate substantially from those of infrequently burned forest.

We use the modelling methodology of Conard et al. (2002) to convert our measurements of burned forest area into estimates of directly emitted carbon. We estimate carbon emissions from Russian forest fires in 2001 to be 32% of those estimated by Conard et al. for 1998. Whilst fire activity is believed to have been significantly more severe in 1998 than in 2001 due to the prevailing meteorological conditions, there is more uncertainty in the Conard et al. estimate because it was derived from AVHRR-based mapping of fires larger than 10 km^2 in only part of Russia, fires in other regions being estimated via adjustments to the official statistics. In contrast, we use a single, standardised methodology to map fires down to 2 km^2 across the entire Russian Federation. We estimate that in 2001, Russia forest fires released five to eight times more carbon than fires in Canadian and Alaskan forests, due primarily to the much larger area affected. Assuming industrial emissions in Russia continued on the same downward trend noted in the 1994–1998 period by Marland, Boden, and Andres (2001), the 39–55 Mt of carbon that we estimate to have been directly released in the 2001 forest fires represents between 11% and 17% of that year's fossil fuel carbon emissions. Clearly, this methodology could be improved with further information on the spatial variability of forest carbon and the relative incidence of surface and crown fires types. However, these results do indicate the significant contribution that fires in the Russian Boreal region make to the global terrestrial carbon budge and data such as these will ultimately be used to improve the accuracy of global biomass burning emissions estimates such as those provided by Andrea and Merlet (2001).

Finally, it is important to note that many of the Russian forest fires detected in this study may well also induce a much longer-term release of carbon, by subjecting permafrost

layers to increased temperatures (due to the removal of overlying shading vegetation) and rates of soil decomposition (Kasischke et al., 1995). Whilst we do not quantify this additional longer-term carbon release here, it could clearly be very significant due to the large amounts of carbon stored in the frozen soils of the Russian boreal region. This further exemplifies the need for good quality, quantitative data on Russian fire activity in order to support improved environmental models of the Russian boreal region. We now plan to map monthly burned area and carbon emissions using VGT for the full 5-year period from 1998 to 2002 in order to obtain better data on the interannual variability of burning, and we will compare these results to simultaneous atmospheric chemistry observations as a further validation exercise.

Acknowledgements

This work is supported via a research grant from the Leverhulme Trust (F/070/40I) and by UK–Russia Exchange funds from the Royal Society. Dr. M.J. Wooster is supported by the NERC Earth Observation Science Initiative. SPOT VGT data are CNES copyright, distributed by SpotImage and produced by VITO.

References

AARS (1999). *Asian Association of Remote Sensing Asia 30-second Land Cover Data Set. CD-ROM.* Japan: AARS-Centre for Environmental Remote Sensing, Chiba University.

Alaska Division of Forestry (2002). Fire management programmes fire statistics. Available at: http://www.dnr.state.ak.us/forestry/firestats.htm. (accessed 25 November 2002).

Alexeyev, V., Birdsey, R. A., Stakanov, V., & Korotkov, I. (1995). Carbon in vegetation of Russian forests: methods to estimate storage and geographical distribution. *Water, Air and Soil Pollution*, *82*, 271–282.

Alexeyev, V. A., & Birdsey, R. A. (1994). *Carbon in ecosystems of forests and peatlands of Russia* (in Russian). Krasnoyarsk, Russia: Sukachev Institute of Forest Research, 170 pp.

Anderson, J. R., Hardy, E. E., Roach, J. T., & Witmer, R. E. (1976). A landuse and land cover classification system for use with remote sensor data. *US Geological Survey Professional Paper, vol. 964*. Washington, DC: USGS, 41 pp.

Andrea, M. O., & Merlet, P. (2001). Emission of trace gases and aerosols from biomass burning. *Global Biogeochemical Cycles*, *15*, 955–966.

Bak, P., Tang, C., & Wiesenfeld, K. (1988). Self-organized criticality. *Physical Reviews A*, *38*, 364–374.

Bourgeau-Chavez, L. L., Harrell, P. A., Kasischke, E. S., & French, N. H. F. (1997). The detecting and mapping of Alaskan wildfires using a spaceborne imaging radar system. *International Journal of Remote Sensing*, *18*, 355–373.

Brown, J. F., Loveland, T. R., Ohlen, D. O., & Zhu, Z. (1999). The global land-cover characteristics database: The users' perspective. *Photogrammetric Engineering and Remote Sensing*, *65*, 1069–1074.

Cahoon, D. R., Stocks, B. J., Levine, J. S., Cofer, W. R., & Barber, J. A. (1996). Monitoring 1992 forest fires in the boreal ecosystem using NOAA AVHRR satellite imagery. In J. S. Levine (Ed.), *Biomass burning and global change* (pp. 795–801). Cambridge, MA: MIT Press.

Conard, S., Sukhinin, A., Stocks, B., Cahoon, D., Davidenko, E., & Ivanova, G. (2002). Determining effects of area burned and fire severity on carbon cycling and emissions in Siberia. *Climatic Change*, *55*, 197–211.

Conard, S. G., & Ivanova, G. A. (1997). Wildfire in Russian Boreal forests—potential impacts of fire regime characteristics on emissions and global carbon balance estimates. *Environmental Pollution*, *98*, 305–313.

Drummond, J. R. (1992). In J. C. Gille, & G. Visconti (Eds.), *Measurements of Pollution in the Troposphere (MOPPIT) in the use of EOS for studies of atmospheric physics* (pp. 77–101). Amsterdam: North-Holland.

Eastwood, J. A., Plummer, S. E., Wyatt, B. K., & Stocks, B. J. (1998). The potential of SPOT-Vegetation data for fire scar detection in boreal forests. *International Journal of Remote Sensing*, *19*, 3678–3681.

Flannigan, M., & Van Wagner, C. (1991). Climate change and wildfire in Canada. *Canadian Journal Forest Research*, *21*, 61–72.

Fraser, R. H., Hall, R. J., & Landry, R. (2001). Burnt area mapping across Canada's boreal forest zone using SPOT VEGETATION calibrated with Landsat TM imagery. *3rd International Workshop on Remote Sensing and GIS Applications to Forest Fire Management* (pp. 133–137). Paris: EARSEL.

Fraser, R. H., & Li, Z. (2002). Estimating fire-related parameters in boreal forest using SPOT VEGETATION. *Remote Sensing of Environment*, *82*, 95–110.

Fraser, R. H., Li, Z., & Cihlar, J. (2000). Hotspot and NDVI Differencing Synergy (HANDS): A new technique for burned area mapping over boreal forest. *Remote Sensing of Environment*, *74*, 362–376.

Fraser, R. H., Li, Z., & Landry, R. (2000). SPOT VEGETATION for characterising boreal forest fires. *International Journal of Remote Sensing*, *21*, 3525–3532.

Fredriksen, P., Lanaas, S., & Mbaye, M. (1990). NOAA-AVHRR and GIS-based monitoring of fire activity in Senegal—a provisional methodology and potential applications. In G. J. Goldammer (Ed.), *Fire in the tropical biota, ecosystem processes and global challenges* (pp. 401–417). Berlin: Springer-Verlag.

Fuller, D. O. (2000). Satellite remote sensing of biomass burning with optical and thermal sensors. *Progress in Physical Geography*, *24*, 543–561.

Goldammer, J. G., & Furyaev, V. V. (1996). Fire in ecosystems of Boreal Eurasia: Ecological impacts and links to the global system. In J. G. Goldammer, & V. V. Furyaev (Eds.), *Fire in ecosystems of Boreal Eurasia* (pp. 1–20). Dordrecht: Kluwer.

Isaev, A. S., Korovin, G. N., Bartalev, S. A., Ershov, D. V., Janetos, A., Kasischke, E. S., Shugart, H. H., French, N. H. F., Orlick, B. E., & Murphy, T. L. (2002). Using remote sensing to assess Russian forest fire carbon emissions. *Climatic Change*, *55*, 235–249.

Johnston, T. (2001). *CIFFC Canada report 2001*. Winnipeg, Canada: Canadian Interagency Forest Fire Centre, 6 pp.

Justice, C. O., Malingreau, J. P., & Setzer, A. W. (1993). Satellite remote sensing of fire: Potential and limitations. In P. Crutzen, & J. Goldhammer (Eds.), *Fire and the environment* (pp. 77–88). New York: Wiley

Kasischke, E. S. (2000). Boreal ecosystems in the global carbon cycle. In E. S. Kasischke, & B. J. Stocks (Eds.), *Fire, climate change and carbon cycling in the boreal forest. Ecological Studies Series* (pp. 19–30). New York: Springer-Verlag.

Kasischke, E. S., Bourgeau-Chavez, L. L., O'Neill, K. P., & French, N. H. F. (2000). Indirect and long-term effects of fire on the boreal forest carbon budget. In J. L. Innes, M. Beniston, & M. M. Verstraete (Eds.), *Biomass burning and its inter-relations with the climate system* (pp. 263–280). Dordrecht, The Netherlands: Kluwer Academic Publishers.

Kasischke, E. S., Christensen, N. L., & Stocks, B. J. (1995). Fire, global warming, and the carbon balance of boreal forests. *Ecological Applications*, *5*, 437–451.

Kasischke, E. S., & French, N. H. F. (1995). Locating and estimating the areal extent of wildfires in Alasksn boreal forests using multi-season AVHRR NDVI composite data. *Remote Sensing of Environment*, *51*, 263–275.

Kasischke, E. S., French, N. H. F., Harrell, P., Christensen Jr., N. L., Ustin, S. L., & Barry, D. (1993). Monitoring of wildfires in boreal forests using large area AVHRR NDVI composite data. *Remote Sensing of Environment*, *44*, 51–71.

Kaufman, Y., & Tanré, D. (1992). Atmospherically Resistant Vegetation Index (ARVI) for EOS-MODIS. *IEEE Transactions on Geoscience and Remote Sensing*, *30*, 261–270.

Li, Z., Nadon, S., & Cihlar, J. (2000). Satellite-based detection of Canadian boreal forest fires: Development and application of the algorithm. *International Journal of Remote Sensing*, *21*, 3057–3069.

Malamud, B. D., Morein, G., & Turcotte, D. L. (1998). Forest fires: An example of self-organized critical behavior. *Science*, *281*, 1840–1841.

Malamud, B. D., & Turcotte, D. L. (2000). Cellular-automata models applied to natural hazards. *IEEE Computing in Science and Engineering*, *2*, 42–51.

Marland, G., Boden, T. A., & Andres, R. J. (2001). Global, regional and national CO_2 emissions. *Trends: A compendium of data on global change*. Oak Ridge, TN: Carbon Dioxide Analysis Centre, Oak Ridge National Laboratory, US Department of Energy. Available at http://cdiac.esd.ornl.gov/trends/emis/em_cont.htm.

Martín, P., & Chuvieco, E. (1993). Mapping and evaluating burned land from multitemporal analysis of AVHRR NDVI images. *Proceedings of the international workshop on satellite technology and GIS for Mediterranean forest mapping and fire management* (pp. 71–83). Thessaloniki, Greece: Department of Forestry and Natural Environment, Aristotle University, 4–6 November.

Oberlander, E. A., Brenninkmeijerm, A. M., Crutzen, P. J., Lelieveld, J., & Elansky, N. F. (2002). Why not take the train? Trans-Siberian atmospheric chemistry observations across Central and East Asia. *EOS Transactions of the American Geophysical Union*, *83*, 509–516.

Passot, X. (2000). VEGETATION image processing methods in the CTIV. *Proceedings of VEGETATION 2000, 2 years of operation to prepare the future, Belgirate, 3–6 April, Italy* (pp. 15–21). Available at http://vegetation.cnes.fr.

Redmond, R. L., Winne, C. J., Opitz, D. W., & Mangrich, M. V. (2002). Classifying and mapping wildfire severity. Imaging notes, 16(5). Space-imaging, CO, USA.

Ricotta, C., Arianoutsou, M., Diaz-Delgado, R., Duguy, B., Lloret, F., Maroudi, E., Mazzoleni, S., Moreno, J., Rambal, S., Vallejo, R., & Vasquez, A. (2001). Self-organized criticality of wildfires ecologically revisited. *Ecological Modelling*, *141*, 307–311.

Ricotta, C., Avena, G. C., & Marchetti, M. (1999). The flaming sandpile: Self-organized criticality and wildfires. *Ecological Modelling*, *119*, 73–77.

Saint, G. (1996). The VEGETATION programme. *The Earth Observer*, *8*(4). Available at http://eospso.gsfc.nasa.gov/eos_observ/7_8_96/P21.html.

Smith, A. M. S., Wooster, M. J., Powell, A. K., & Usher, D. (2002). Texture based feature extraction: Application to fire scar detection in Earth Observation Imagery. *International Journal of Remote Sensing*, *23*, 1733–1739.

Stocks, B. J., & Lynham, T. J. (1996). Fire weather climatology in Canada and Russia. In J. G. Goldammer, & V. V. Furyaev (Eds.), *Fire in ecosystems of Boreal Eurasia* (pp. 481–487). The Netherlands: Kluwer Academic Publisher.

Stroppiana, D., Pinnock, S., Pereira, J. M. C., & Gregoire, J. M. (2002). Radiometric analysis of SPOT-VEGETATION images for burnt area detection in Northern Australia. *Remote Sensing of Environment*, *82*, 21–37.

Van Cleve, K., Oliver, R., Schlentner, L., Viereck, L. A., & Dyrness, C. T. (1983). Productivity and nutrient cycling in taiga forest ecosystems. *Canadian Journal of Forest Research*, *13*, 747–766.

Weber, M. G., & Stocks, B. J. (1998). Forest fires and sustainability in the boreal forests of Canada. *Ambio*, *27*, 545–550.

Wotawa, G., Novelli, P. C., Trainer, M., & Granier, C. (2001). Inter-annual variability of summertime CO concentrations in the Northern Hemisphere explained by boreal forest fires in North America and Russia. *Geophysical Research Letters*, *28*, 4575–4578.